Nano Energy 53 (2018) 958–966

Contents lists available at ScienceDirect

Nano Energy

journal homepage: www.elsevier.com/locate/nanoen

Full paper

Interface engineering of sulfide electrolytes for all-solid-state lithium batteries

Ruochen Xu[a,b], Fudong Han[a], Xiao Ji[a], Xiulin Fan[a], Jiangping Tu[b,*], Chunsheng Wang[a,*]

[a] Department of Chemical and Biomolecular Engineering, University of Maryland, College Park, MD 20742, United States
[b] State Key Laboratory of Silicon Materials, Key Laboratory of Advanced Materials and Applications for Batteries of Zhejiang Province, and School of Materials Science& Engineering, Zhejiang University, Hangzhou 310027, China

ARTICLE INFO

Keywords:
Sulfide solid electrolyte
Lithium metal anode
Lithium dendrites
Interface modification
Lithium ion battery

ABSTRACT

All-solid-state lithium batteries (ASSLIBs) employing sulfide solid electrolyte hold high promise to replace traditional liquid-electrolyte LIBs due to their high safety and energy density. However, Li dendritic growth in sulfide electrolyte limits the realization of the high energy of ASSLIBs. In this work, we use LiF (or LiI) layer at the interface between Li and sulfide electrolyte and penetrated HFE (or I solution) inside of sulfide electrolyte to suppress the Li dendrite growth. Due to the higher interface energy of LiF/Li than that of LiI/Li, LiF interlayer show much higher capability than LiI in suppressing the Li dendrite. Even if the Li dendrite breaks through LiF (or LiI) interlayer, the Li dendrites will be consumed by coated/penetrated HEF (or I) forming LiF (or LiI) thus preventing Li dendrite growth. A $LiNbO_3$ @$LiCoO_2$/$Li_7P_3S_{11}$/Li ASSLIB employing HFE coated/infiltrated $Li_7P_3S_{11}$ glass-ceramic as electrolyte, and LiF coated Li metal as anode shows a high reversible discharge capacity of 118.9 mAh g^{-1} at 0.1 mA cm^{-2} and retains 96.8 mAh g^{-1} after 100 cycles. The designed solid electrolyte interphase between Li and solid electrolyte that has a high interface energy to Li provides new opportunity to commercialize the Li metal batteries.

1. Introduction

Lithium metal is recognized as the optimal choice for anode material to achieve high energy density batteries because it has low negative electrochemical potential (−3.04 V *vs.* standard hydrogen electrode), low density (0.53 g cm^{-1}) and high theoretical capacity (3860 mAh g^{-1}) [1,2]. However, lithium metal is extremely reactive and it is easy to form uncontrolled dendritic lithium at the interface of lithium anode, which may puncture the separator during cycles, thus leading to internal short-circuiting and serious safety issues [3]. In the past decades, various attempts have been made to suppress Li dendrite growth by introducing electrolyte additives [4], forming protective films [5] and employing Li-hosted current collectors [6]. However, it is still far away from the practical realization for Li metal-based batteries. Bulk-type all-solid-state lithium batteries (ASSLIBs) employing mechanically-strong solid electrolytes hold the promise to suppress the lithium dendrite and achieve high energy density [7–11]. To realize the highly promising solid electrolyte batteries, the solid electrolyte should satisfy the following requirements: (1) high ionic conductivity of > 1.0 mS cm^{-1} at room temperature, (2) wide electrochemical window (> 5.0 V *vs.* Li/Li^+), (3) negligible electron conductivity, (4) high chemical compatibility *versus* anodes and cathodes. However, most highly-conductive sulfide-type solid electrolytes (such as $Li_7P_3S_{11}$, 17 mS cm^{-1} [12]; $Li_{10}GeP_2S_{12}$, 12 mS cm^{-1} [13]; $Li_{9.54}Si_{1.74}P_{1.44}S_{11.7}Cl_{0.3}$, 25 mS cm^{-1} [14].) have an unstable interface against lithium metal [14–16]. Another key challenge is the formation of Li dendritic along the voids and grain boundaries in these solid electrolytes [17] although these materials have much stronger mechanical strength than Li metal. In fact, the Li dendrite is more easily grown in sulfide solid electrolytes than in liquid electrolytes with unknown mechanism.

Li dendrite formation in sulfide electrolytes are closely related to the interface stability of the electrolyte with Li. Most sulfide electrolytes are not stable with Li. During Li plating at a potential below 0.0 V, these sulfide electrolytes will be reduced forming a solid interphase layer. Although the reduction of the electrolytes can enhance the wettability of the electrolyte with Li anode, it also increases the interface resistance because the interphase layer normally has a lower ionic conductivity than the parent electrolyte [18]. If the interphase has a low interface energy with Li anode or has a high electronic conductivity, the interphase will promote the Li dendrite growth. For example, the decomposition of $Li_{10}GeP_2S_{12}$ when contacting with Li will largely reduce the

* Corresponding authors.
E-mail addresses: tujp@zju.edu.cn (J. Tu), cswang@umd.edu (C. Wang).

https://doi.org/10.1016/j.nanoen.2018.09.061
Received 15 August 2018; Received in revised form 14 September 2018; Accepted 25 September 2018
Available online 27 September 2018

ionic conductivity of solid electrolytes due to the poor conducting interphase. [19]. Since the reduction interphase layer (Li_2S, Li_3P, and $Li_{15}Ge_4$ [16]) has much lower ionic conductivity and higher electronic conductivity than $Li_{10}GeP_2S_{12}$, the high interface resistance and low limiting current for Li dendrite formation limit the application of Li metal anode in $Li_{10}GeP_2S_{12}$. To minimize electrochemical reduction of sulfide electrolytes, lithium alloys with a high alloying/dealloying potential have been used as an anode. Li-In alloy with a flat voltage plateau at 0.62 V (*vs.* Li/Li^+) for In-Li_x ($0 < x < 0.9$) and a high specific capacity [20] has been widely used in ASSLIBs to suppress the reduction interface reactions of solid electrolytes. However, Li-In alloy anodes significantly reduced the cell energy density due to the reduced cell voltage and capacity. In addition, the expensive of indium metal also increases the cell cost. Therefore, enhancing the interfacial stability between lithium metal and sulfide solid electrolytes to suppress the Li dendrite growth is critical for the utilization of sulfide electrolytes in solid state Li batteries [21–23].

The interface stability of the electrolytes with Li metal and the nature of formed interphase affects the Li dendrite formation in the electrolytes. However, the mechanism for dendrite formation and growth in solid electrolyte is unclear and controversial [24]. Using *situ* SEM, Nagao et al. [17] reported that lithium initially reacts and grow along grain boundaries and the cracks inside the sulfide electrolyte. However, the Li dendrite still form and grow in grain-boundary free amphoras sulfide electrolytes [25]. To suppress the Li dendrite growth, the interface reaction with Li has to be prohibited by a solid electrolyte interphase and the interphase layer should have a high interface energy.

In this work, we demonstrate that the interfacial reactions between lithium metal and $Li_7P_3S_{11}$ sulfide solid electrolytes (LPS) and Li dendrite are significantly suppressed by LiF (or LiI) interphase layer. LiF and LiI layers are electrochemically stable with both solid electrolytes and Li. They also have high interface energy with Li [26]. By coating methoxyperfluorobutane (HFE) (or I) on the surface and infiltrating HFE (or I) into the holes among sulfide solid electrolyte particles, the LiF or LiI interphase layer on the interface between Li anode and sulfide electrolyte can prevent the Li dendrite growth. Even if the lithium dendrite passed through the LiF (or LiI) interphase layer, it can quickly react with penetrated HFE (or I), consuming Li and suppressing the growth of dendrite. The Li-Li symmetrical cell using LiF coated Li and HFE infiltrated sulfide electrolyte can be stably charge/discharged for 200 cycles without Li dendrite formation in the room temperature at a current of 0.5 mA cm^{-2} and a capacity of 0.1 mAh cm^{-2}. Coupled with a $LiNbO_3$ (LNO) coated $LiCoO_2$ (LCO) cathode, ASSLIBs with LiF layer coated and HFE infiltrated sulfide electrolyte exhibits a high capacity of 118.9 mAh g^{-1} for 100 cycles. The LiF layer coating combing with F-rich solvent infiltrating to electrolytes is a universal strategy for stabilizing the Li/electrolyte interface and preventing the growth of lithium dendrite for high-performance ASSLIBs.

2. Results and discussion

The schematic diagram of $Li/Li_7P_3S_{11}$ interface of ASSLIBs is illustrated in Fig. 1a. The bare lithium metal directly contacts with $Li_7P_3S_{11}$ sulfide solid electrolytes, forming a decomposition layer consisting of Li_2S and Li_3P at interface due to the chemical instability of $Li_7P_3S_{11}$ against lithium metal [15,27,28]. As a result, the high interfacial resistance restricts the fast transport of lithium ions and promoting the Li dendrite formation/growth, limiting use of sulfide electrolytes for Li metal batteries [29,30]. Therefore, our strategy is to coat a uniform LiF (or LiI) thin layer on lithium metal by exposing Li metal to HFE (or I_2) and also infiltrating HFE (or I) into sulfide electrolytes to prevent the Li dendrite growth (Fig. 1b). As a result, we realized improved interfacial stability, which was demonstrated by long cycle stability of chronoamperometry charge/discharge of lithium symmetric cells and $Li/Li_7P_3S_{11}/LiCoO_2$ full cells.

LiF or LiI is formed on Li surface on Li after exposing Li to HFE and I_2 gas at 150 °C. Fig. 2a shows the schematic diagrams of the processes for the surface coating of LiF (or LiI) layer on the Li metal surface. When Li is exposed to HFE (or I_2) gas, it will spontaneously react with Li metal and form a layer on the surface. To prove the successful coating of LiF (or LiI) layer on lithium metal, we conduct the analysis using X-ray diffraction (XRD), scanning electron microscopy (SEM) and energy dispersive X-ray photoelectron spectroscopy (XPS). Fig. 2b shows the XRD patterns of the prepared LiF and LiI coated Li, where the diffraction peaks of LiF and Li for LiF@Li and LiI and Li for LiI@Li are clearly observed, confirming that the LiF (or LiI) coating layer successfully grew on the lithium foils. The lithium oxide peaks observed in the XRD is formed during preparation and measurement since the Li foils have been polished before the experiments. The scanning electron microscope (SEM) images of polished pristine Li are shown in Fig. S1. Fig. 2c, d show the SEM images of the top surface of LiI-coated and LiF-coated Li foils obtained by exposing Li metal to I_2 or HFE gases at 150 °C for 6 h, respectively. The surface of LiI-coated Li foil exhibits very rough morphology with several pores (Fig. 2c), while the LiF-coated Li foil shows dense and less rough surface morphology (Fig. 2d). It is because the large volume expansion of 200% from Li to LiI increases the roughness of the formed LiI surface, while the volume change from Li to LiF is extremely small (−15%). Fig. S2 shows that the thickness of the LiF and LiI coated layers are approximately 1.08 μm and 1.31 μm, respectively. In addition, the X-ray photoelectron spectroscopy (XPS) results (Fig. 2e, f, g) further confirmed that the LiF-rich layer and pure LiI layer were successfully coated on Li. As shown in Fig. 2e, the peak at 684.90 eV is originated from the signal of F 1s [31,32], which confirms the growth of LiF film on the Li foil, in agreement with the XRD analysis. The C 1s XPS signal of Li@LiF (Fig. 2f) shows four peaks at 284.80, 286.70, 287.70, 292.50, attributed to C-C, C-O bands, and CF, CF_2 groups, respectively [33,34]. The CF and CF_2 groups are generated from the reactions between Li and HFE. As for the Li@LiI sample, two peaks at 618.90 and 630.40 eV in the I 3d spectra (Fig. 2g) were assigned to the characteristic peaks of I^- [35], confirming the successful preparation of LiI coated Li metal.

$Li_7P_3S_{11}$ was synthesized by high-energy mechanical ball milling with follow-up annealing. All the diffraction peaks in X-ray diffraction (XRD) pattern of the $Li_7P_3S_{11}$ solid electrolyte (Fig. S3a) are identified to characteristic peaks of $Li_7P_3S_{11}$ [36,37], conforming a highly pure $Li_7P_3S_{11}$ was synthesized. Sharp diffraction peaks imply a high crystallinity of the as-synthesized electrolytes. The Raman spectrum between the wavelengths of 300–500 cm^{-1} were also used to characterization of $Li_7P_3S_{11}$ electrolyte. Two main peaks at 405 cm^{-1} and 420 cm^{-1} in Fig. S3b are assigned to the stretching of $P_2S_7^{4-}$ and PS_4^{3-} respectively [38], confirming the existence of $Li_7P_3S_{11}$. From the XRD and Raman characterizations, $Li_7P_3S_{11}$ glass-ceramics structure is shown in Fig. S4. The $Li_7P_3S_{11}$ glass-ceramics have the *P*-1 space group with a three-dimensional network consisting of Li − Li bonds around the P_2S_7 di-tetrahedral and PS_4 tetrahedral units [27,39]. The structural framework of $Li_7P_3S_{11}$ crystal facilitates the high mobility of Li ions due to the low potential barrier, making it a promising solid electrolyte with high conductivity for ASSLIBs. SEM results (Fig. S5) show that the $Li_7P_3S_{11}$ electrolyte particles are uniform size of around 2–5 μm. The ionic conductivity of $Li_7P_3S_{11}$ is measured using a blocking $Pt/Li_7P_3S_{11}/Pt$ cell. As is shown in Fig. S6, the synthesized $Li_7P_3S_{11}$ electrolyte has a high lithium ion conductivity of 1.89 mS cm^{-1} at room temperature with an activation energy of 227 meV, which is comparable with the value of the reported $Li_7P_3S_{11}$ sulfide solid electrolytes [15,40].

Fig. S7 shows the SEM images of the surface of $Li_7P_3S_{11}$ electrolyte after cold pressing. Some micropores and cracks can be observed on the solid electrolyte. The width of the cracks is around 500–800 nm and the size of the micropores is in the range of 200–500 nm. The SEM images (Fig. S8) of cross-section further confirm that cracks and pores exist in the entire electrolyte pellet. The cracks and pores promote lithium dendrite growth along these cracks and pores during repeated

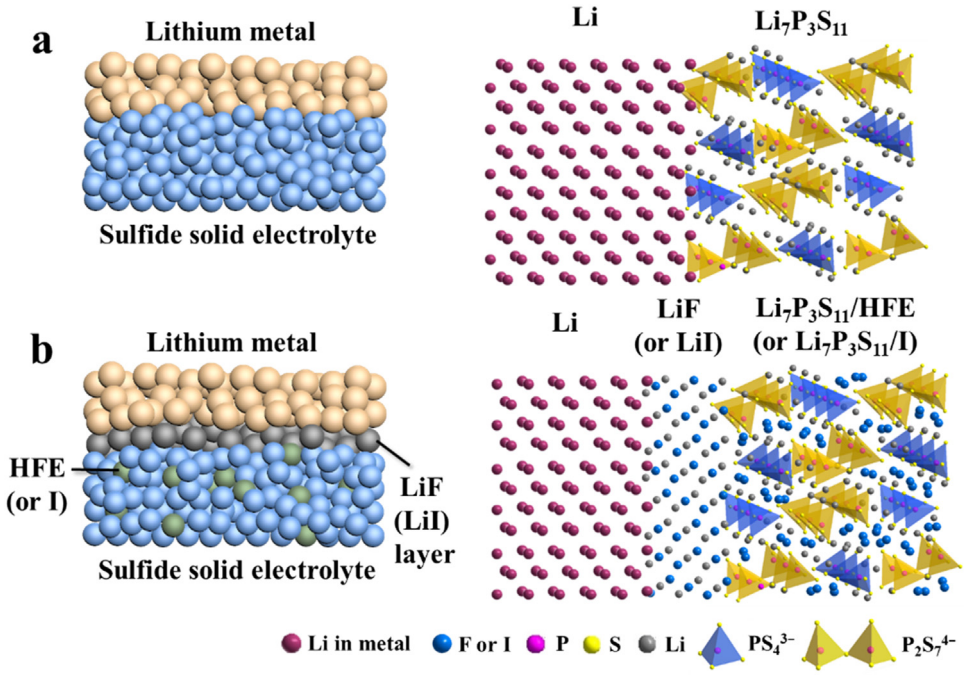

Fig. 1. Schematic diagrams of (a) Li/$Li_7P_3S_{11}$ interface of ASSLIBs and (b) modified interface with a uniform thin LiF (or LiI) interphase layer and HFE (or I solution) infiltrated sulfide electrolyte.

stripping/plating cycles, as shown in Fig. 3a. To suppress the Li dendrite growth, HFE (or I) solutions is coated on the surface and also infiltrated into these cracks and pores of solid electrolyte, where Li can react with HFE (or I) forming LiF (or LiI) even if the Li dendrite breaks the coated LiF (or LiI) layer. The LiF (or LiI) interphase layer ensures the stability/compatibility at lithium/electrolyte interface and inhibits the growth of lithium dendrite simultaneously (Fig. 3b). Therefore, the advantage of this method is that the infiltrated HFE (or I) in electrolyte will consume the lithium dendrite by formation of LiF (or LiI) at boundaries and in cracks and thus prevents the Li dendrite growth in the micro-short circuit of ASSLIBs.

The effect of LiF and LiI interphase layer on the interface resistance and Li dendrite suppression were evaluated in a symmetrical Li/electrolyte/Li cells using LiF (or LiI) coated Li, and HFE (or I) coated/infiltrated $Li_7P_3S_{11}$ electrolyte. The interfacial resistance was evaluated by electrochemical impedance spectroscopy (EIS). The LiF (or LiI) coated Li foils were pressed on the both side of the solid electrolyte for 24 h to ensure the stability between Li and electrolyte before testing. If the LiF is broken during assembly of the symmetric Li@LiF/$Li_7P_3S_{11}$(HFE)/LiF@Li, the HFE will penetrate into the crack and react with Li forming LiF. Three symmetric cells, Li/LPS/Li (Bare Li cell), Li@LiI/LPS(I)/LiI@Li (LiI coated cell) and Li@LiF/LPS(HFE)/LiF@Li (LiF coated cell), were synthesized in an argon-filled glove box. The EIS profiles of the symmetric cells are shown in Fig. 3c. The resistance in the intersection at the high-frequency range is attributed to the solid electrolyte, while semi-circle resistance can be attributed to the interface resistances between Li and electrolyte [41]. As shown in Fig. 3c, the bulk resistances of $Li_7P_3S_{11}$ in three cells are approximately 82.8 $\Omega\,cm^{-2}$ due to the same thickness of the electrolytes. However, the Li cell using bare electrolyte exhibits a high interfacial resistance of about 127.4 $\Omega\,cm^{-2}$ due to the decomposition reaction of $Li_7P_3S_{11}$ to Li_2S and Li_3P. The interfacial resistance reduces to 66.2 $\Omega\,cm^{-2}$ and 48.4 $\Omega\,cm^{-2}$ for the cells using LiI and LiF coated Li metals, respectively. The results indicate that the LiF and LiI interphase between Li and electrolyte effectively suppressed the side reactions and dramatically reduces the interfacial resistance.

The capability of LiF and LiI interphases in suppressing Li dendrite growth was evaluated by galvanostatic discharge/charge cycles at a fixed stripping/plating capacity of 0.1 mAh cm^{-2} at room temperature. As shown in Fig. 3d and g, at a low current density of 0.1 mA cm^{-2}, Li cell using a bare electrolyte exhibits curved overpotential with a high average overpotential of about 25 mV, which is much larger than that of LiI coated cell (about 18 mV) and LiF coated cell (about 12 mV) during entire 200 cycles. At a high current of 0.2 mA cm^{-2} (Fig. 3e, h), the bare Li cell shows a large increase in polarization followed by internal short circuit after 110 cycles due to the growth of lithium dendrite. The LiI coated cell also shows short circuit after 150 cycles while LiF coated cell does not short after 200 cycles. As the current density further increased to 0.5 mA cm^{-2} (Fig. 3f, i), the LiF coated cell still remained stable and a low overpotential in entire 200 cycles. It exhibits an average overpotential of 90 mV with a low total resistance of 293.0 $\Omega\,cm^{-2}$. In contrast, the polarization of the bare Li cell increases dramatically to 0.3 V. Both the bare Li cell and LiI coated cell suffer internal short circuit after 54 and 116 cycles, respectively, due to the lithium dendrite propagation. When a higher current density of 1.0 mA cm^{-2} was applied to the symmetric cells at room temperature (Fig. S9), the LiF coated cell is still able to keep stable over 60 cycles despite large polarization occurs, which is significantly better than bare Li cell with extremely high polarization followed by internal short circuit after 12 cycles. The LiI coated cell only survives for 18 cycles at such a high current density.

The electrochemical performance and EIS analysis of three symmetric Li/Li cells using bare Li metal, LiF or LiI coated Li metals demonstrated that interface resistance of bare Li metal cell quickly increases and the cell rapidly failed during Li plating/striping especially at a high current due to reduction of LPS by lithium. The formed interphase layer has a poor ionic conductivity at Li/$Li_7P_3S_{11}$ interface, resulting in a high interfacial resistance. The side reaction also promotes the Li dendrite growth in the LPS electrolyte, resulting in quick short circuit. LiI and LiF with high stability to Li and $Li_7P_3S_{11}$ are chosen as the SEI layer between Li and $Li_7P_3S_{11}$ to prevent the reduction of sulfide electrolytes due to the extremely low electronic conductivity [24,26,34,42]. In addition, the LiF SEI layers are able to suppress the dendrite due to high interface energy between Li and LiF. In comparison, LiF is easier to form dense/uniform layer on lithium metal and possesses high stability window over 6 V *vs.* Li/Li^+ [43], thus

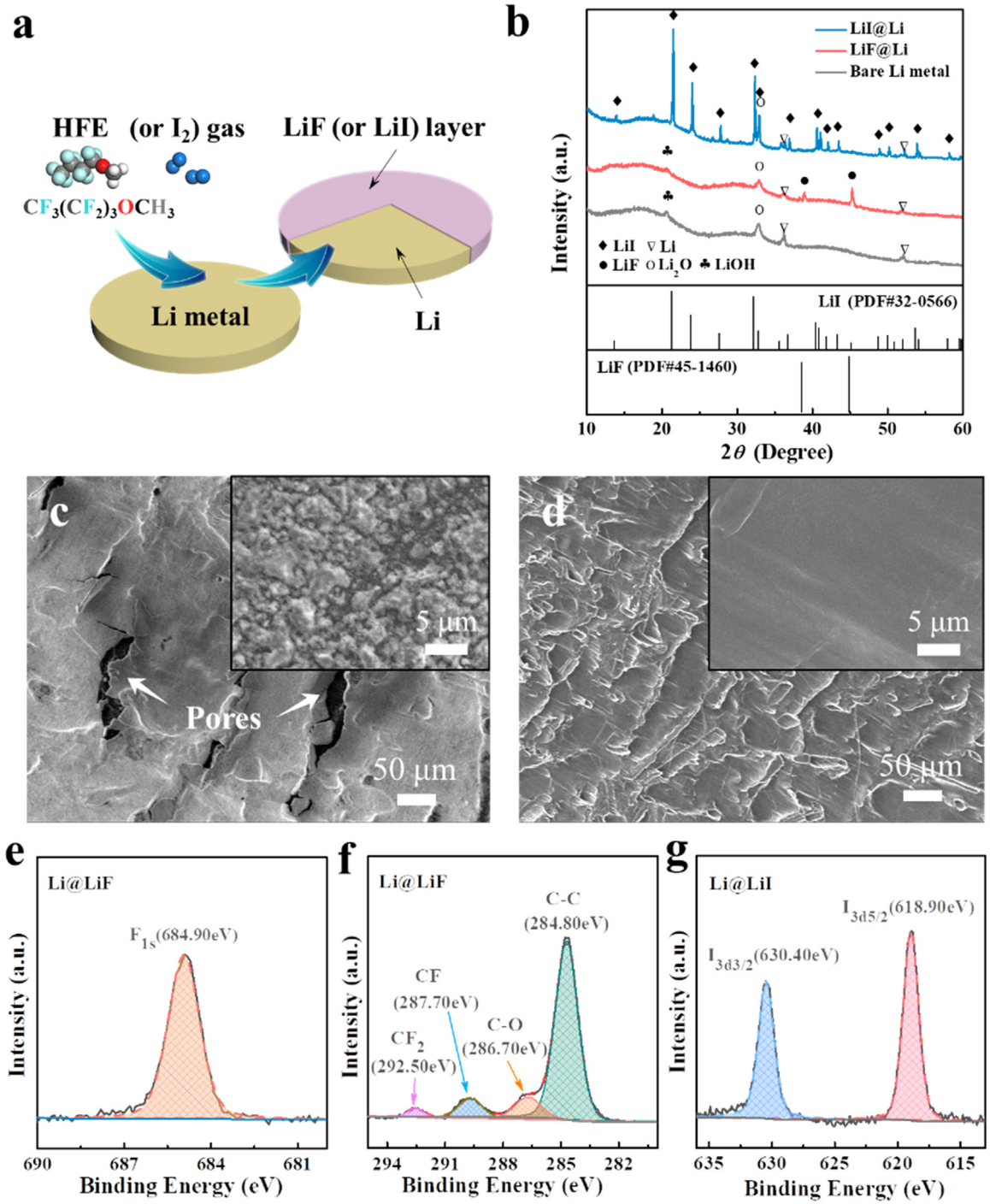

Fig. 2. (a) Schematic diagrams of the processes for the surface coating of LiF (or LiI) layer on the Li metal surface. (b) XRD patterns of the prepared Li@LiI (bule line), Li@LiF (red line) and Li metal (black line). SEM images of the top surface of (c) Li@LiI and (d) Li@LiF foils. XPS detail spectra of (e) F 1s and (f) C 1s for Li@LiF and (g) I 3d for Li@LiI.(For interpretation of the references to color in this figure legend, the reader is referred to the web version of this article).

it has advantages over LiI in maintaining interface stability and inhibiting the growth of lithium dendrite [26], which is supported by the electrochemical performance of symmetrical cells. Even if Li dendrite passes through LiF interphase layer and grows into LPS electrolyte through grain boundaries/cracks, it quickly reacts with HFE (or I) forming LiF (or LiI), consuming the lithium dendrite in sulfide solid electrolyte and extending the cycle lives.

The interface stability at $Li/Li_7P_3S_{11}$, Li/LiF and Li/LiI were also calculated using density functional theory (DFT). The interface energy was first calculated using DFT to understand the interface stability and the Li dendrite suppression capability. DFT calculation in Fig. 4a shows that the interface energy linearly changes with the number of Li. The interface energy values (γ) at $Li/Li_7P_3S_{11}$, Li/LiF and Li/LiI can be obtained from the vertical axis intercept. Fig. 4b shows DFT calculated interface energy of each compound to Li. The negative interface energy at the $Li/Li_7P_3S_{11}$ interface demonstrates the instability between Li metal and $Li_7P_3S_{11}$ electrolyte [15,44]. LiI and LiF both show positive interface energy *versus* Li metal. Therefore, LiI and LiF are highly stable to Li. In addition, the Li/LiF interface has much higher interface energy (73.28 meV $Å^{-2}$) than Li/LiI interface (36.67 meV $Å^{-2}$). The high interface energy at Li/LiF improves the Li diffusion along the Li/LiF interface, relieves interface stress and promotes a uniform Li deposition

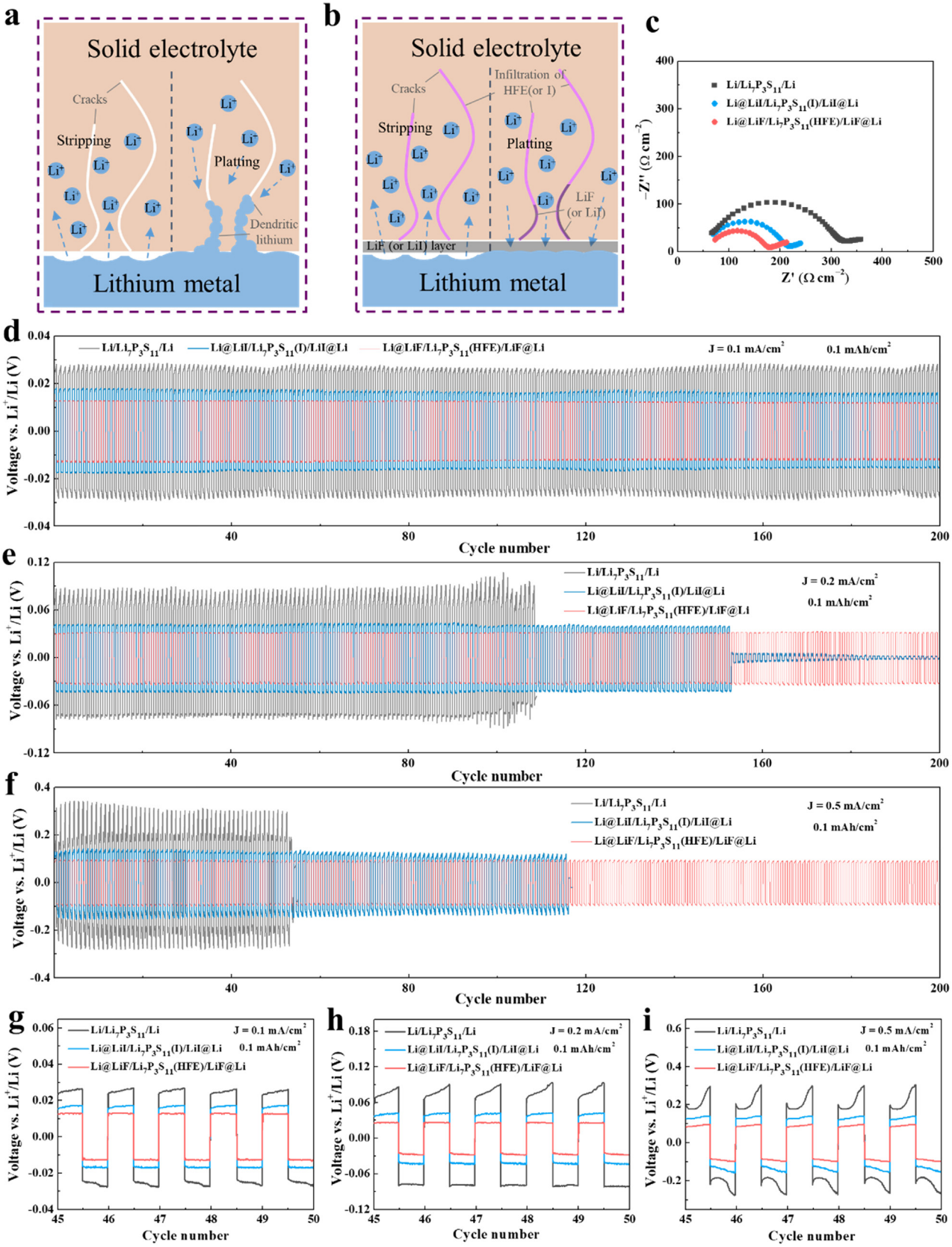

Fig. 3. Schematic diagrams of lithium stripping/plating behavior of (a) bare Li with untreated solid electrolyte and (b) LiF (or LiI) coated Li metal with HFE (or I) infiltrated electrolyte. (c) Nyquist plots of Li/LPS/Li, Li@LiI/LPS(I)/LiI@Li and Li@LiF/LPS(HFE)/LiF@Li symmetrical cells. Galvanostatic discharge/charge voltage profiles of Li/LPS/Li (black), Li@LiI/LPS(I)/LiI@Li (blue) and Li@LiF/LPS(HFE)/LiF@Li (red) symmetrical cells at current densities of (d, g) 0.1 mA cm^{-2}, (e, h) 0.2 mA cm^{-2}, and (f, i) 0.5 mA cm^{-2} with a fixed stripping/plating capacity of 0.1 mAh cm^{-2} at room temperature. (For interpretation of the references to color in this figure legend, the reader is referred to the web version of this article).

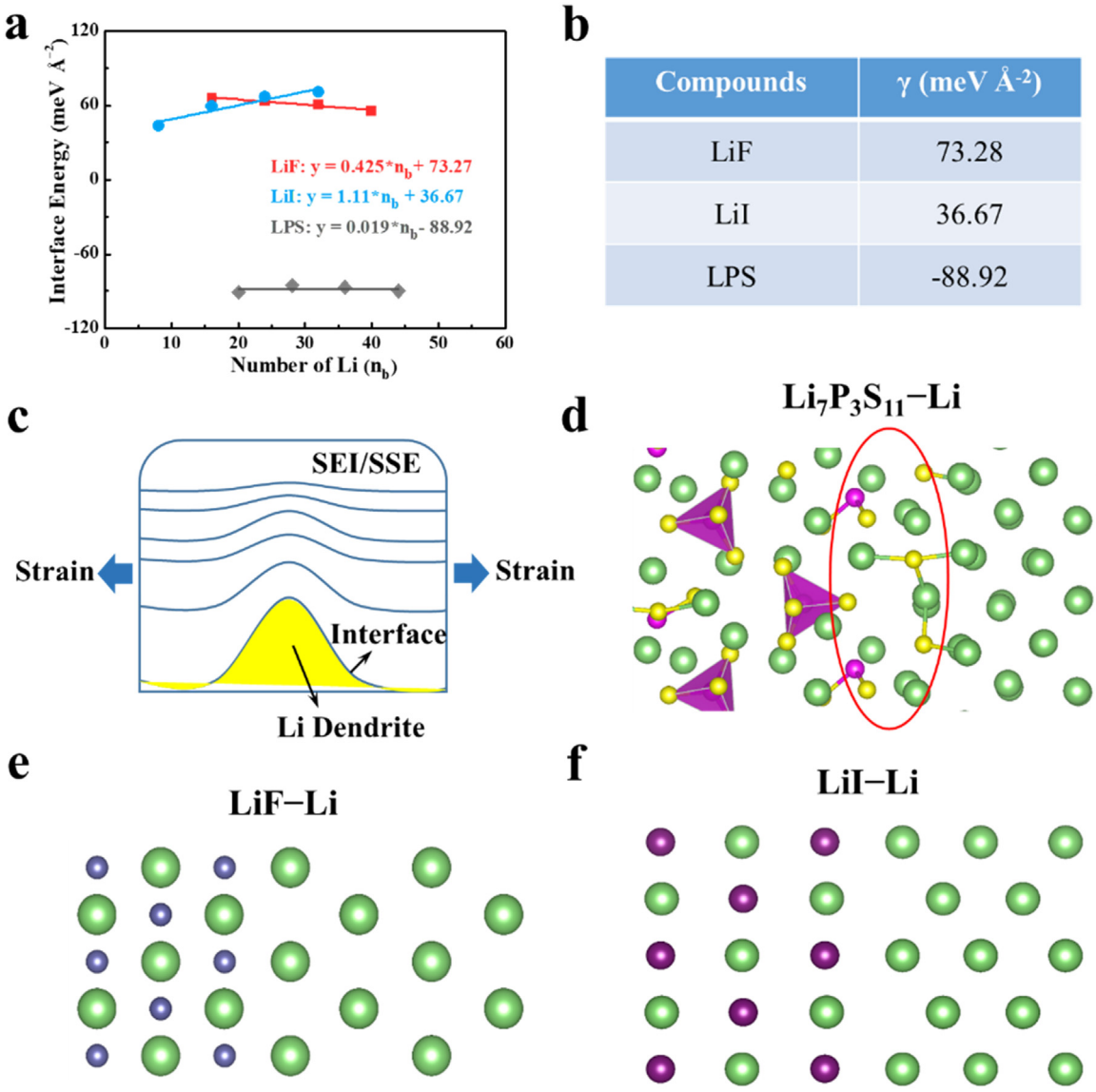

Compounds	γ (meV Å^{-2})
LiF	73.28
LiI	36.67
LPS	-88.92

Fig. 4. (a) DFT calculation results between the interface energy and the number of Li at $Li_7P_3S_{11}$/Li, LiF/Li and LiI/Li. The interface energy values can be obtained from the vertical axis intercept. (b) DFT calculated interface energy values (γ) of $Li_7P_3S_{11}$, LiF and LiI to Li. (c) Schematic diagram of Li deposition with LiF layer. The interfaces structure at (d) Li/$Li_7P_3S_{11}$, (e) Li/LiF and (f) Li/LiI.

(Fig. 4c). Therefore, LiF layer can suppress dendrite growth. The interfaces structure at Li/$Li_7P_3S_{11}$, Li/LiF and Li/LiI that are built based on the surface energy and construction rules are shown in Fig. 4d, e and f, respectively. The relaxed Li/$Li_7P_3S_{11}$ interface undergoes the large distortion near the interfacial region, which exacerbates the interface reactions. In contrast, the relaxed Li/LiF and Li/LiI interfaces experience very good matching.

Using $LiNbO_3$ coated $LiCoO_2$ (LNO@LCO) as a cathode, the electrochemical performances of the all-solid-state sulfide electrolyte Li/LCO full cell were examined. The high $LiCoO_2$ loading of 3.6 mg cm^{-2} was used in the all-solid-state cell to achieve high energy density. Fig. 5a shows the first three charge-discharge curves of the Li/LPS/LCO cell (Bare Li/LCO cell) at the current density of 0.1 mA cm^{-2} at room temperature in the voltage of 2.5–4.2 V. The cell exhibits the initial charge capacity of 143.2 mAh;g^{-1} and the corresponding discharge capacity of 106.4 mAh g^{-1}. The low Coulombic efficiency in the first cycle is attributed to the reaction between LCO and LPS. The sulfide solid electrolyte materials are not thermodynamically stable at the voltage of 4 V [28]. A high polarization and quick capacity decline are observed in the following cycles. Fig. 5b and c shows the galvanostatic charge-discharge profiles of the Li@LiI/LPS(I)/LCO cell (LiI@Li/LCO cell) and Li@LiF/LPS(HFE)/LCO cell (LiF@Li/LCO cell) at 0.1 mA cm^{-2}, respectively. Comparing the two cells, the total capacity of LiF@Li/LCO cell is higher than that of LiI@Li/LCO cell, which is because the dense LiF layer is uniformly coated on lithium metal and the full cell resistance is much lower due to the thin LiF layer (Fig. S10). A high reversibility and a low polarization can be observed in the LiF@Li/LCO cell due to the suppression of side reactions. Fig. 5d presents the cycling performances of the Li/LCO cell, LiI@Li/LCO cell and LiF@Li/LCO cell at 0.1 mA cm^{-2}. The initial discharge capacity of LiF@Li/LCO cell is 118.9 mAh g^{-1} and the reversible capacity stabilizes at about 100 mAh g^{-1} after 20 cycles. The discharge capacity at 100th cycle still retains 96.8 mAh g^{-1} with a capacity retention of 81.4%. In contrast, the bare Li/LCO cell and LiI@Li/LCO cell only exhibits 77.5 and 51.2 mAh g^{-1} after 100 cycles, respectively. With the help of LiF coating and infiltrated HFE in sulfide solid electrolyte, the LiF@Li/LCO cell shows the best performance with high capacity and long cycle stability (Fig. 5e), which is consistent with the results of the symmetrical Li/electrolyte/Li cell test. The electrochemical impedance spectroscopy (EIS) results (Fig. S10) also prove that the resistance of LiF@

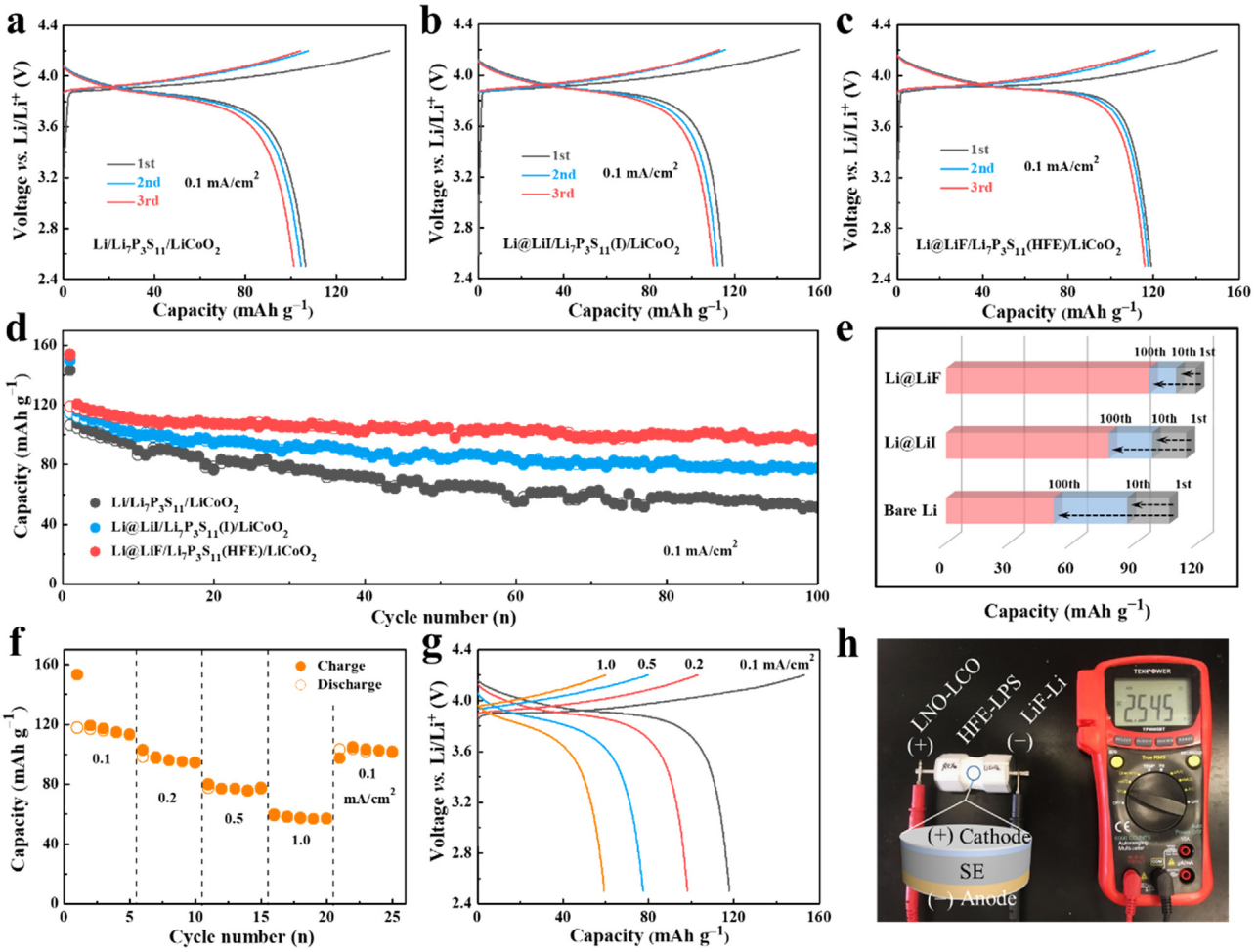

Fig. 5. Charge-discharge profiles of the (a) Li/LPS/LCO cell, (b) Li@LiI/LPS(I)/LCO cell and (c) Li@LiF/LPS(HFE)/LCO cell at current density of 0.1 mA cm^{-2} at room temperature. (d) Cycling performance of assembled ASSLIBs at 0.1 mA cm^{-2}. (e) Comparison of the capacity retention data at 1st, 10th and 100th cycles. (f) Rate performance of Li@LiF/LPS(HFE)/LCO ASSLIB at various current densities from 0.1 mA cm^{-2} to 1.0 mA cm^{-2} at 25 °C. (g) Charge-discharge curves of Li@LiF/LPS(HFE)/LCO cell under different current densities. (h) The open-circuit of a Li@LiF/LPS(HFE)/LCO cell before testing and inset is the schematic diagram of the configuration of the all-solid-state cell.

Li/LCO is much smaller than the other two counterpart Li/LCO cells, mainly due to the highly stable Li/electrolyte interface that effectively suppresses Li dendrite. The rate capabilities of the LiF@Li/LCO cell were also evaluated at current densities from 0.1 mA cm^{-2} to 1.0 mA cm^{-2} at 25 °C (Fig. 5f, g). The discharge specific capacities of the LiF@Li/LCO cell at the current densities of 0.1, 0.2, 0.5, 1.0 mA cm^{-2} are 117.8, 98.2, 77.4 and 59.2 mAh g^{-1}, respectively, which demonstrates the excellent rate performance. When the current density decreases back to 0.1 mA cm^{-2}, the capacity can return back to 103.2 mAh g^{-1}, indicating that the LiF cell is stable at a high current density up to 1.0 mA cm^{-2}. The assembled Li/LCO all-solid-state cell that is composed of LNO@LCO cathode, HFE infiltrated LPS solid electrolyte and LiF@Li anode has an open-circuit of 2.545 V (Fig. 5h).

The outstanding electrochemical performance of LiF@Li/LCO cell can be ascribed to the high capability of LiF layer at the Li/$Li_7P_3S_{11}$ surface and at $Li_7P_3S_{11}$ particle-to-particle in suppressing the Li dendrite. In addition to suppress the Li dendrite, the formation of LiF also consume the Li dendrite self-healing the cell. The optimization of thickness LiF and controlling amount of coated and infiltrated HFE can further enhance the electrochemical performance.

3. Conclusion

In summary, we demonstrate that the LiF interfacial layer at Li/$Li_7P_3S_{11}$ interface and infiltration of HFE into $Li_7P_3S_{11}$ can greatly suppress the Li dendrite formation in $Li_7P_3S_{11}$ thus enhancing the electrochemical performance. Even if the Li dendrite breaks the LiF layer and penetrates into $Li_7P_3S_{11}$. The reaction of penetrated Li with HFE will consume the Li and also prevent the followed Li penetration due to high interface energy of LiF with Li. The assembled Li@LiF/$Li_7P_3S_{11}$/LiF@Li symmetrical cell can stably plating/stripping at 0.5 mA cm^{-2} and 0.1 mAh cm^{-2} at 25 °C for over 200 cycles, confirming a super capability of LiF in suppressing Li dendrite. Coupled with the LNO-LCO cathode, the all-solid-state Li@LiF/$Li_7P_3S_{11}$/LNO@LCO full cell exhibits a high initial reversible capacity of 118.9 mAh g^{-1} with excellent cycling stability and high rate performances at room temperature. The interface engineering strategy paves the way for practical application of high-performance all-solid-state lithium secondary batteries.

4. Experimental section

4.1. Sample synthesis

$Li_7P_3S_{11}$ sulfide solid electrolyte was prepared *via* a high-energy mechanical ball milling technique and subsequent heat treatment process. Li_2S (Sigma-Aldrich, 99.98%), P_2S_5 (Sigma-Aldrich, 99%) were used as starting materials, which were mixed with the stoichiometric

proportion of Li_2S: P_2S_5 = 7: 3 in an argon filled glove box. The powder was placed in a zirconia pot (50 mL) and ball-milled (PM 100, Retsch) at 510 rpm for 40 h at room temperature. The obtained powder was sealed in a vacuum quartz tube and then heated at a temperature of 250 °C for 2 h in a furnace to enable the crystallization of solid electrolytes. To coat LiF layer on Li metal, Li foil was polished and cut into pieces with the diameter of 10 mm. The Li pieces were placed above the surface of methoxyperfluorobutane solvent (HFE, Sigma-Aldrich, 99.9%) in an argon-filled reactor. And the reactor was sealed and heated at 150 °C for 6 h. When the reaction was complete, the LiF-coated Li metal was obtained. Similarly, LiI-coated Li metal was also prepared. The Li pieces and I_2 powder (Sigma-Aldrich, 99.99%) were sealed in a quartz tube, then heated at a temperature of 150 °C for 6 h. When preparing solid cells with LiF-coated Li metal, HFE is infiltrated in $Li_7P_3S_{11}$ electrolytes. Firstly, $Li_7P_3S_{11}$ powder (120 mg) was put in a PTFE tank with a diameter of 10 mm and then cold pressed under 360 MPa for 3 min. Then, HFE was quickly added into solid electrolyte pellets using a pipette and the amount of liquid was controlled (≈ 0.1 mL), then the cells are sealed with parafilm to prevent HFE from volatilizing. As for the preparation of $Li_7P_3S_{11}$ electrolytes penetrated I solution, a I solution was prepared by dissolving the I_2 powder (10 mg) in 1,2-dimethoxyethane (DME) (1 mL, Sigma-Aldrich, 99%). The infiltration I solution into $Li_7P_3S_{11}$ solid electrolytes ($Li_7P_3S_{11}$(I)) was carried out by adding the I solution (≈ 0.1 mL) into electrolyte pellets in an argon-filled glovebox.

4.2. Materials characterization

X-ray diffraction (XRD) measurements were carried out by a D8 Advance with LynxEye and Solx (Bruker AXS, WI, USA) with Cu Kα line as radiation source. Raman spectra were recorded on a Horiba Jobin Yvon Labram Aramis using a 532 nm diode-pumped solid-state laser. The morphologies of the samples were obtained using a Hitachi a SU-70 field-emission scanning electron microscope (SEM). X-ray photoelectron spectroscopy (XPS) was tested using a Kratos Axis 165 spectrometer with a monochromatic Al Kα X-ray radiation source.

4.3. Electrochemical measurement

The ionic conductivities of synthesized $Li_7P_3S_{11}$ electrolyte were measured using electrochemical impedance spectroscopy (EIS) by a blocking symmetric Pt/$Li_7P_3S_{11}$/Pt cell. The as-synthesized $Li_7P_3S_{11}$ powder (150 mg) was cold-pressed under 360 MPa with the thickness of around 1 mm in a PTFE tank (10 mm in diameter). Pt was sputtering on both sides of the pellets. The temperature was controlled between 25 and 105 °C in a temperature chamber. The non-blocking symmetric Li/$Li_7P_3S_{11}$/Li cell was assembled in an argon-filled glove box. In addition, the Li@LiI/$Li_7P_3S_{11}$(I)/LiI@Li, and Li@LiF/$Li_7P_3S_{11}$(HFE)/LiF@Li symmetric cells were synthesized for the chronoamperometry test.

All-solid-state lithium cells were fabricated by employing $LiNbO_3$@$LiCoO_2$/$Li_7P_3S_{11}$ composite as cathode, $Li_7P_3S_{11}$ infiltrated HFE (or I) as solid electrolyte and LiF-coated (or LiI-coated) Li metal as anode. The $LiNbO_3$ coated $LiCoO_2$ ($LiNbO_3$@$LiCoO_2$) was used as the active material. Composite electrodes consist of $LiNbO_3$@$LiCoO_2$ and $Li_7P_3S_{11}$ with a weight ratio of 70: 30 were prepared by hand-grinding in the mortar. For the assembly of all-solid-state cells, the $LiNbO_3$ @$LiCoO_2$/$Li_7P_3S_{11}$ power (4 mg) were uniformly spread onto one side of the $Li_7P_3S_{11}$ solid electrolyte (120 mg) in a PTFE tank with a diameter of 10 mm, and cold-pressed together under the 360 MPa. The loading of active material on the electrode is around 3.6 mg cm^{-2}. The HFE (or I) solutions was added into $Li_7P_3S_{11}$ electrolytes from the other side. After that, a LiF-coated Li foil (or LiI-coated Li) was pressed on the other side of the solid electrolyte as a counter and reference electrode. Finally, the three-layered pellet was attached with two stainless steel disks as current collectors. All the preparation processes were performed in a dry argon-filled glovebox (O_2 < 0.1 ppm, H_2O < 0.1 ppm). The EIS measurements were carried out at frequencies from 1 MHz to 0.1 Hz with the AC amplitude of 20 mV by an electrochemistry workstation (Solatron 1287/1260). The galvanostatic discharge-charge cycles were tested using an Arbin BT2000 workstation (Arbin Instruments, TX, USA) in a voltage of 2.5–4.2 V at room temperature. Applied currents and charge-discharge capacities were calculated on the basis of the weight of $LiCoO_2$ in the cathode.

Acknowledgements

This work is supported by the U.S. Department of Energy ARPA-E (Award No. DE-AR0000781) and Army Research Office (Program Manager: Dr. Robert Mantz) under Award No. W911NF1510187.

Conflict of interest

The authors declare no competing financial interest.

Appendix A. Supplementary material

Supplementary data associated with this article can be found in the online version at doi:10.1016/j.nanoen.2018.09.061.

References

[1] D. Lin, Y. Liu, Y. Cui, Nat. Nanotechnol. 12 (2017) 194–206.
[2] K.K. Fu, Y.H. Gong, B.Y. Liu, Y.Z. Zhu, S.M. Xu, Y.G. Yao, W. Luo, C.W. Wang, S.D. Lacey, J.Q. Dai, Y.N. Chen, Y.F. Mo, E. Wachsman, L.B. Hu, Sci. Adv. 3 (2017) e1601659.
[3] Y. Gao, Y. Zhao, Y.C. Li, Q. Huang, T.E. Mallouk, D. Wang, J. Am. Chem. Soc. 139 (2017) 15288–15291.
[4] X.Q. Zhang, X.B. Cheng, X. Chen, C. Yan, Q. Zhang, Adv. Funct. Mater. 27 (2017) 1605989.
[5] N.W. Li, Y.X. Yin, C.P. Yang, Y.G. Guo, Adv. Mater. 28 (2016) 1853–1858.
[6] G. Zheng, S.W. Lee, Z. Liang, H.W. Lee, K. Yan, H. Yao, H. Wang, W. Li, S. Chu, Y. Cui, Nat. Nanotechnol. 9 (2014) 618–623.
[7] C.W. Sun, J. Liu, Y.D. Gong, D.P. Wilkinson, J.J. Zhang, Nano Energy 33 (2017) 363–386.
[8] Z. Gao, H. Sun, L. Fu, F. Ye, Y. Zhang, W. Luo, Y. Huang, Adv. Mater. 30 (2018) 1705702.
[9] E. Rangasamy, Z. Liu, M. Gobet, K. Pilar, G. Sahu, W. Zhou, H. Wu, S. Greenbaum, C. Liang, J. Am. Chem. Soc. 137 (2015) 1384–1387.
[10] Y. Wang, W.D. Richards, S.P. Ong, L.J. Miara, J.C. Kim, Y. Mo, G. Ceder, Nat. Mater. 14 (2015) 1026–1031.
[11] D.H. Kim, D.Y. Oh, K.H. Park, Y.E. Choi, Y.J. Nam, H.A. Lee, S.M. Lee, Y.S. Jung, Nano Lett. 17 (2017) 3013–3020.
[12] Y. Seino, T. Ota, K. Takada, A. Hayashi, M. Tatsumisago, Energy Environ. Sci. 7 (2014) 627–631.
[13] N. Kamaya, K. Homma, Y. Yamakawa, M. Hirayama, R. Kanno, M. Yonemura, T. Kamiyama, Y. Kato, S. Hama, K. Kawamoto, A. Mitsui, Nat. Mater. 10 (2011) 682–686.
[14] Y. Kato, S. Hori, T. Saito, K. Suzuki, M. Hirayama, A. Mitsui, M. Yonemura, H. Iba, R. Kanno, Nat. Energy 1 (2016) 16030.
[15] S. Wenzel, D.A. Weber, T. Leichtweiss, M.R. Busche, J. Sann, J. Janek, Solid State Ion. 286 (2016) 24–33.
[16] S. Wenzel, S. Randau, T. Leichtweiß, D.A. Weber, J. Sann, W.G. Zeier, J. Janek, Chem. Mater. 28 (2016) 2400–2407.
[17] M. Nagao, A. Hayashi, M. Tatsumisago, T. Kanetsuku, T. Tsuda, S. Kuwabata, Phys. Chem. Chem. Phys. 15 (2013) 18600–18606.
[18] A.C. Luntz, J. Voss, K. Reuter, J. Phys. Chem. Lett. 6 (2015) 4599–4604.
[19] F.D. Han, Y.Z. Zhu, X.F. He, Y.F. Mo, C.S. Wang, Adv. Energy Mater. 6 (2016) 1501590.
[20] K. Takada, N. Aotani, K. Iwamoto, S. Kondo, Solid State Ion. 86 (1996) 877–882.
[21] A. Kato, A. Hayashi, M. Tatsumisago, J. Power Sources 309 (2016) 27–32.
[22] Z. Zhang, S. Chen, J. Yang, J. Wang, L. Yao, X. Yao, P. Cui, X. Xu, ACS Appl. Mater. Interfaces 10 (2018) 2556–2565.
[23] N.S. Choi, Z. Chen, S.A. Freunberger, X. Ji, Y.K. Sun, K. Amine, G. Yushin, L.F. Nazar, J. Cho, P.G. Bruce, Angew. Chem. Int. Ed. Engl. 51 (2012) 9994–10024.
[24] F. Han, J. Yue, X. Zhu, C. Wang, Adv. Energy Mater. (2018) 1703644.
[25] L. Porz, T. Swamy, B.W. Sheldon, D. Rettenwander, T. Frömling, H.L. Thaman, S. Berendts, R. Uecker, W.C. Carter, Y.M. Chiang, Adv. Energy Mater. 7 (2017) 1701003.
[26] Y. Lu, Z. Tu, L.A. Archer, Nat. Mater. 13 (2014) 961–969.
[27] I.H. Chu, H. Nguyen, S. Hy, Y.C. Lin, Z. Wang, Z. Xu, Z. Deng, Y.S. Meng, S.P. Ong, ACS Appl. Mater. Interfaces 8 (2016) 7843–7853.
[28] Y. Zhu, X. He, Y. Mo, ACS Appl. Mater. Interfaces 7 (2015) 23685–23693.
[29] F. Han, T. Gao, Y. Zhu, K.J. Gaskell, C. Wang, Adv. Mater. 27 (2015) 3473–3483.
[30] A. Manthiram, X.W. Yu, S.F. Wang, Nat. Rev. Mater. 2 (2017) 16103.

[31] T. Aytun, A. Turak, I. Baikie, G. Halek, C.W. Ow-Yang, Nano Lett. 12 (2012) 39–44.
[32] Z.S. Wu, L. Xue, W. Ren, F. Li, L. Wen, H.M. Cheng, Adv. Funct. Mater. 22 (2012) 3290–3297.
[33] J.T. Robinson, J.S. Burgess, C.E. Junkermeier, S.C. Badescu, T.L. Reinecke, F.K. Perkins, M.K. Zalalutdniov, J.W. Baldwin, J.C. Culbertson, P.E. Sheehan, E.S. Snow, Nano Lett. 10 (2010) 3001–3005.
[34] D. Lin, Y. Liu, W. Chen, G. Zhou, K. Liu, B. Dunn, Y. Cui, Nano Lett. 17 (2017) 3731–3737.
[35] S. Kim, S.K. Kim, P. Sun, N. Oh, P.V. Braun, Nano Lett. 17 (2017) 6893–6899.
[36] F. Mizuno, A. Hayashi, K. Tadanaga, M. Tatsumisago, Adv. Mater. 17 (2005) 918–921.
[37] M.R. Busche, D.A. Weber, Y. Schneider, C. Dietrich, S. Wenzel, T. Leichtweiss, D. Schröder, W. Zhang, H. Weigand, D. Walter, S.J. Sedlmaier, D. Houtarde, L.F. Nazar, J. Janek, Chem. Mater. 28 (2016) 6152–6165.
[38] Y. Wang, D. Lu, M. Bowden, P.Z. El Khoury, K.S. Han, Z.D. Deng, J. Xiao, J.G. Zhang, J. Liu, Chem. Mater. 30 (2018) 990–997.
[39] H. Yamane, M. Shibata, Y. Shimane, T. Junke, Y. Seino, S. Adams, K. Minami, A. Hayashi, M. Tatsumisago, Solid State Ion. 178 (2007) 1163–1167.
[40] X. Yao, D. Liu, C. Wang, P. Long, G. Peng, Y.S. Hu, H. Li, L. Chen, X. Xu, Nano Lett. 16 (2016) 7148–7154.
[41] K.K. Fu, Y. Gong, Z. Fu, H. Xie, Y. Yao, B. Liu, M. Carter, E. Wachsman, L. Hu, Angew. Chem. Int. Ed. Engl. 56 (2017) 14942–14947.
[42] J. Zhao, L. Liao, F. Shi, T. Lei, G. Chen, A. Pei, J. Sun, K. Yan, G. Zhou, J. Xie, C. Liu, Y. Li, Z. Liang, Z. Bao, Y. Cui, J. Am. Chem. Soc. 139 (2017) 11550–11558.
[43] W.D. Richards, L.J. Miara, Y. Wang, J.C. Kim, G. Ceder, Chem. Mater. 28 (2015) 266–273.
[44] N. Lepley, N. Holzwarth, N. Phys. Rev. B 92 (2015) 214201.

Ruochen Xu started his Ph.D. degree in Zhejiang University. He is currently a joint Ph.D. candidate at Department of Chemical and Biomolecular Engineering, University of Maryland-College Park. His research interest is mainly focused on the solid electrolytes for all-solid-state batteries.

Dr. Fudong Han received his Ph.D. degree in Department of Chemical and Biomolecular Engineering, University of Maryland-College Park, and is currently a post-doctoral researcher in Chunsheng Wang's group at University of Maryland. His research focuses on all-solid-state lithium-ion batteries with the aim to minimize the interfacial

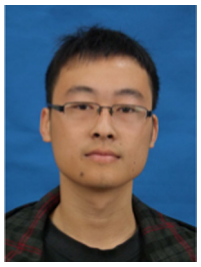

Xiao Ji started his Ph.D. degree in Electronic Science and Technology, Huazhong University of Science and Technology. He is currently a joint Ph.D. candidate at Department of Chemical and Biomolecular Engineering, University of Maryland-College Park. His research interest is mainly focused on First-principles calculations Li-ion batteries and supercapacitor.

Dr. Xiulin Fan received his bachelor's degree and Ph.D. degree both in Materials Science and Engineering from Zhejiang University. He is currently an assistant research scientist at University of Maryland-College Park. His research interests are novel materials, novel electrolytes and their application in energy storage and conversion devices including lithium-ion batteries, sodium-ion batteries and hydrogen storage.

Prof. Jiangping Tu received his Ph.D. degree from Zhejiang University in 1994. From 1998–2000, he worked as a Japan Society for the Promotion of Science (JSPS) research fellow at the Department of Chemical Engineering of Hiroshima University, Japan. He has been a full professor in the school of Materials Science and Engineering at Zhejiang University since 2000. His main research interests are the fabrication and tribological properties of nanocomposites and nanocomposite coatings, novel electrochemical energy storage materials and solid electrolyte materials.

Prof. Chunsheng Wang is a full professor at University of Maryland College Park (UMCP). He was educated in materials science and trained in electrochemistry and got his Ph.D. degree from Zhejiang University. He has more than 150 peer-reviewed journal publications and more than 25 years of experience in battery research. His Li ion battery research has been highlighted in EFRC news by DoE in 2012, and by Chemical & Engineering News in 2013. He is a recipient of the University of Maryland Outstanding Junior Researcher Award.